*Int. J. Electrochem. Sci.*, 7 **(2012)** 2389 - 2402

**International Journal of ELECTROCHEMICAL SCIENCE**
www.electrochemsci.org

# Corrosion Behavior of Ti-6Al-4V Alloys

*C.G. Nava-Dino*[1], C. López-Meléndez[1,2], *R. G. Bautista-Margulis*[3], *M. A. Neri-Flores*[1], *J.G. Chacón-Nava*[1], *S.D de la Torre*[4], *J.G. Gonzalez-Rodriguez*[5] *and A. Martínez-Villafañe*[1,*]

[1] Departamento de Integridad y Diseño de Materiales Compuestos. Centro de Investigación en Materiales Avanzados. S.C. CIMAV. Miguel de Cervantes No. 120, Complejo Industrial Chihuahua, C.P 31109, Chihuahua, Chihuahua, México.
[2]Universidad La Salle Chihuahua. Prolongación Lomas de Majalca No. 11201 Col. Labor de Terrazas C.P. 31020 Chihuahua, Chih. México.
[3] Universidad Juárez Autónoma de Tabasco, División Académica de Ciencias Biológicas, C.P. 86040, Villahermosa, Tabasco, México.
[4] Centro de Investigación e Innovación Tecnológica (CIITEC)-IPN, D.F. México, Cerrada de Cecati S/N, Col. Santa Catarina Azcapotzalco, CP 02250, México D.F.
[5] Centro de Investigación en Ingeniería y Ciencias Aplicadas-UAEM, Av. Universidad 1001, Col. Chamilpa, 62210-Cuernavaca, Morelos, MEXICO.
[*]E-mail: martinez.villafane@cimav.edu.mx

*Received:* 13 January 2012 / *Accepted:* 9 February 2012 / *Published:* 1 March 2012

The alloy Ti-6Al-4V has been considered ideal for implant applications. Electrochemical tests were made to analyze their resistance and predictability to corrosion from green dust samples, SPS (Spark Plasma Sintering) samples and commercial alloying. The corrosion behavior in Ringer´s and Hank´s solution was evaluated by SEM (Scanning Electron Microscope). Fractal dimension were used to study corrosion behavior and corrosion predictability was observed by modeling studies.

**Keywords:** Fractal features, Modeling studies, Electrochemical, Powder metallurgy, SPS

## 1. INTRODUCTION

Titanium and its alloys have been used in orthopedic prostheses; the success of these alloys is based on their excellent corrosion resistance and biocompatibility. Corrosion resistance of titanium and their alloys was tested in Ringer´s, Hank´s solution, saline solution and other physiological media. The formation of protective oxide layer on its surface permits part of the corrosion resistance.

Different surface modifications have been employed to provide a specific resistance to the implants corrosion, these surface modifications mainly consists of physical coating process on the metals involving ceramic materials, such Bioglass, Cerabone and A/W glass ceramic. Titanium

implants, which must work as load-bearinf parts, are commonly coated with a plasma-sprayed hydroxyapatite layer [1]. Ti-based alloys are considered to be good materials for implants because the passive film formed is not very reactive[2].Titanium offers advantages such as good mechanical properties as well as corrosion resistance under biological fluid conditions, although material high cost is a holdup[3]. This research work is focused to find out the weakness in Ti-6Al-4V since this alloy was made by mechanical milling and sintering process.

## 2. MATERIALS AND METHODS

### *2.1 Materials and experimental procedure*

Raw materials (Alfa Aesar): titanium (99.5% purity), aluminum (99.5%), vanadium (99.5%) powders, were prepared by milling the corresponding quantity of metal powder in a high energy SPEX 8000M connected to a hardened steel container with 13mm(Ø) balls as milling media, under inert Ar atmospheres.

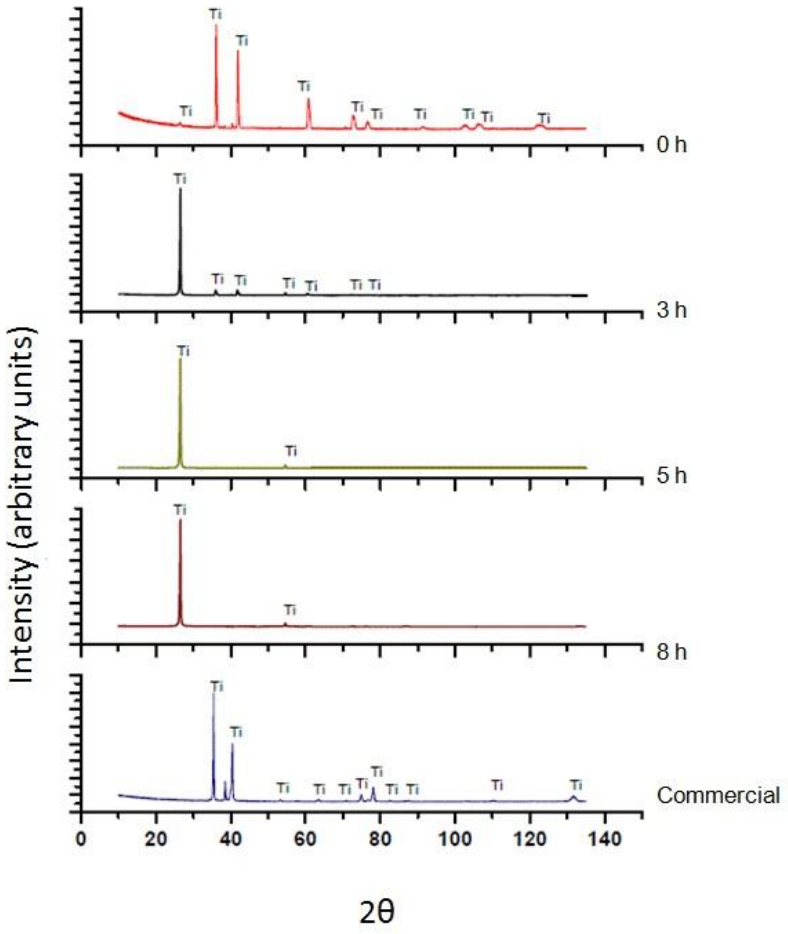


**Figure 1.** X-ray diffraction pattern of the Ti-6Al-4V samples 0, 3, 5, 8 h made by SPS and commercial.

The milling ball to powder weight ratio was kept 5 to 1 for all experimental runs. Methanol was used as process control agent (PCA-1 ml). Milling intervals were 0, 3, 5 and 8 h using alternate cycles of 30 min milling and 30 min resting to protect samples from overheating, using the same milling device for 1 h with the addition of 3 drops of methanol as PCA in order to avoid excessive agglomeration. Green (consolidated) products were obtained by pressing milled powders into a circular die at 950MPa under uniaxial load.

Pressed samples were mounted, polished and etched using standard metallographic techniques in order to carry out the microstructural observations by using a scanning electron microscope JEOL-5800-LV. Hardness tests were carried out in a Wilson Rockwell Instron hardness meter, obtaining values in Vickers scale. Chart average value of 3 indentations and its standard error were present.

The diffraction profiles were measured by a Philips X'pert powder diffractometer using a Cu cathode (= 0.15406 nm). The step size and step time were 0.0334 and 50 s, respectively. X-ray diffraction peak profile analysis was carried out to determine the crystallite size distribution and the dislocation substructure. The differences between Ti-6Al-4V samples by commercial and SPS sintering by 0, 3, 5 and 8 hours were observed according to figure 1.

### *2.2 Preparation of the simulated biofluids*

Alloy used in this study was in the form of bottom of 5g of powder, with composition of Al 6, V 4 y Ti in balance. The Ti-6Al-4V rod was polished (Silicon carbide paper 1200). The total surface of the electrode of Ti-6Al-4V was coated with epoxy resin. The electrode was rinsed in Hank´s and Ringer´s solution. The Hank´s solution was prepared by adding: (in g/l) 8 NaCl, 0.14 CaCl2, 0.4 KCl, 0.35 NaHCO3, 1Glucose, 0.1 $NaH_2PO_4$, 0.1 $MgCl_2.6H_2O$, 0.06 $Na_2HPO_4.2H_2O$ y 0.06 $MgSO_4.7H_2O$ to distilled water[4]. Ringer´s solution have a chemical composition (in g/l) 9NaCl, 0.24 $CaCl_2$, 0.43 KCl and 0.2 $NaHCO_3$ [5, 6, 7].

The Ti-6Al-4V samples were immersed in Ringer´s and Hank´s solution for one hour for stabilization and the open circuit potential was measured during this period with a multimeter, the OCP (Open Circuit Potentials) of the samples were in average -740 and -270 V vs. SCE for 0 to 8 h milling in Hank´s solution. In case of Ringer´s solution has an OCP -700 and –375 V vs. SCE. Commercial samples in Hank´s solution has in average -280 and -270 mV vs. SCE, in Ringer´s solution -0.446V and -0.317 vs. SCE. The samples offer better corrosion resistance in Hank´s solution than Ringer´s. The electrochemical corrosion behavior in cyclic polarization was performed. Analysis was done according with ASTM G1 and ASTM G59.

### *2.3 Morphological characterization*

The surface morphology of the samples were analyzed using scanning electron microscope (SEM) before immersion in Hank´s and Ringer´s solution of green samples in a) 0, b) 3, c) 5 and d) 8hours of milling time and SPS sintering samples in 0, 3, 5 and 8h, samples. The samples are clean and polished to see their composition; in Figure 2 they are shown without electrochemical analysis. Figure

3 shows the commercial alloy Ti-6Al-4V with EDS (Energy Dispersive Spectrometer) analysis; EDS analysis reflects the clean and pure composition of Ti-6Al-4V. SEM images were taken for their analysis by fractal dimension, the feasibility of the two-dimensional R/S analysis was tested with synthetic matrices representing fractional surfaces. In this work, the MATLAB software FRACLAB 2.03 developed by INRIA (http://www.irccyn.ec-nantes.fr/hebergement/FracLab) was used to understand the corrosion behavior of the samples and COMSOL multiphysics version 4.1 to corrosion predictability by electrochemical module.

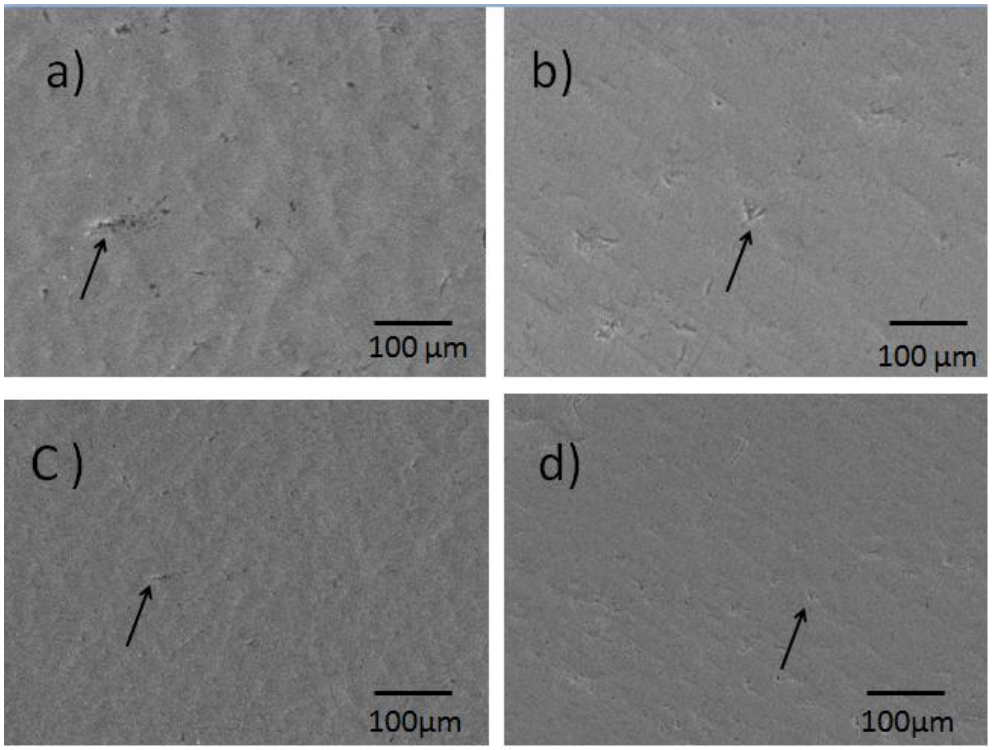


**Figure 2.** SEM micrograph of Ti-6Al-4V powders milled for (a) 0, (b) 3, (c) 5 and (d) 8h; after SPS sintering porous were observed.

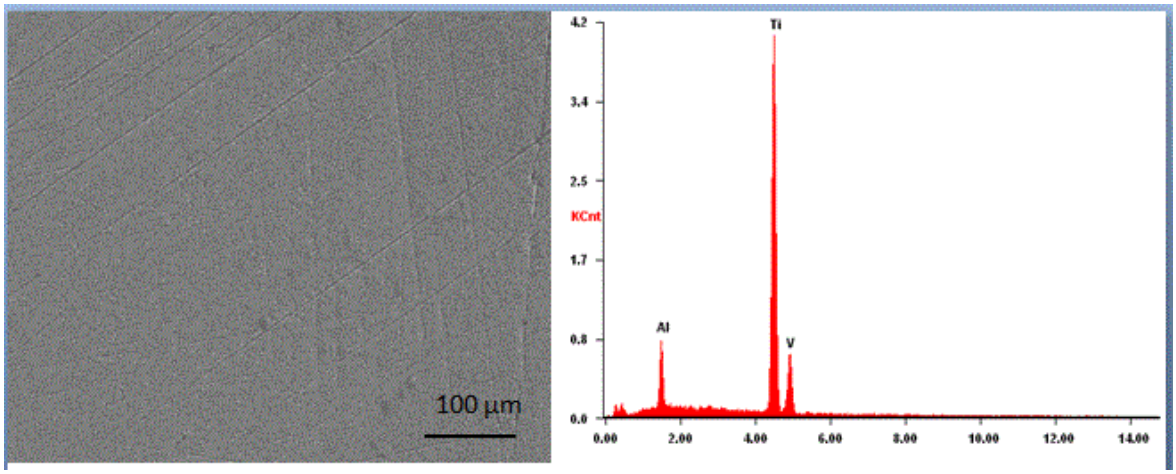


**Figure 3.** SEM image and EDS spectra of Ti-6Al-4V commercial samples.

SEM images were used by other researchers as a resource in some medical or graphical applications that require the transformation of objects while preserving their topology. This, in turn, leads to the well-known notion of a simple point: a point in a binary image. The notion of a simple point is fundamental for all transformations where some topological features are to be preserved [8]. Digital image correlation (DIC) is a whole-field and noncontact deformation measuring method that could provide deformation information of a specimen by processing two digital images that are captured before and after the deformation [9].

### *2.4. Electrochemical characterization*

Corrosion is defined as an electrochemical process in which a solid metal interacts with its chemical environment leading to a loss of substance from the material [4]. Corrosion has been conducted by potentiodynamic polarization (Tafel analysis) made by green samples of Ti-6Al-4V. Such results may determine the corrosion behavior of the samples after they are sintering.

## 3. RESULTS AND DISCUSSION

### *3.1. Characterization analysis*

**Table 1.** Variation of microhardness of Ti-6Al-4V made by SPS and commercial

| Milling intensity [h] SPS | Microhardness [Vickers] |
|---|---|
| 0 | 238 Hv |
| 3 | 246 Hv |
| 5 | 259 Hv |
| 8 | 263 Hv |
| Commercial | 685 Hv |

The results of microhardness in SPS and commercial samples are shown in table 1. The average microhardness of Ti-6Al-4V was found to be 246 Hv, however, in the case of commercial samples were higher than the SPS samples. The graphics of microhardness were listed in figure 4; the graphic shows the increment of value with the increment of the milling time. Microhardness test was done by green samples of materials with 5 grams of weight, and compacted in 5 seconds with 10 ton; then the samples were sintering by SPS. The repeatability was done with 3 indentations mounted in resin. The microstructure reveals the presence of porous or some dominant phase.

To understand part of the samples behavior in Ringer´s and Hank´s solution, an artificial salts mixture was usually used in combination with naturally occurring body substances (blood serum, tissue extracts) and/or more complex chemically defined nutritive solutions for culturing animal cells. Some analysis show the SEM, EDXS and XPS results revealing that, in the case of polished and

passivated samples, after exposure to Hank´s solution, a layer of CaH (PO4) _2H2O has been formed at the surface of the steel [10].

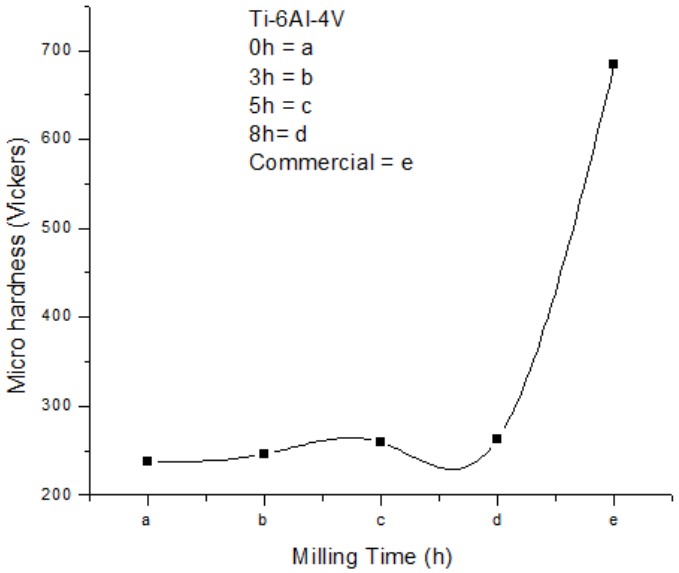


**Figure 4.** Microhardness Ti-6Al-4V with milling time for samples sintering by SPS and commercial

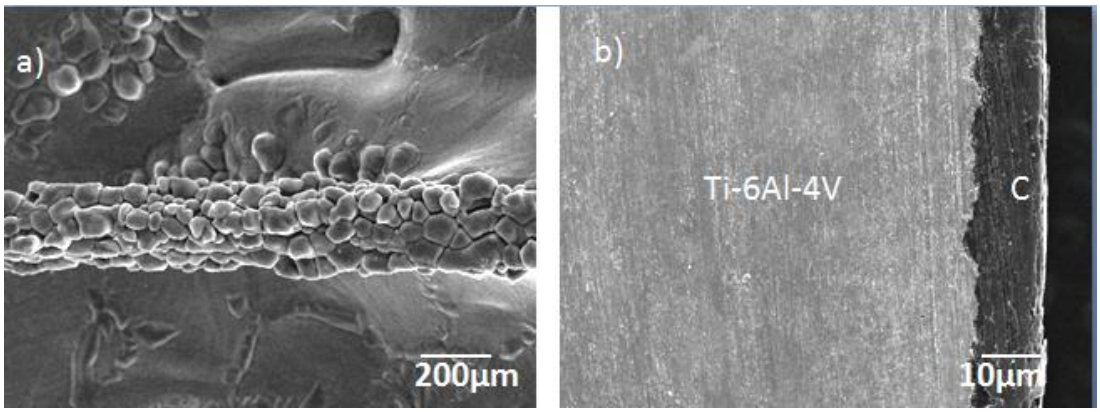


**Figure 5.** SEM micrographs revealing the granular morphology of carbon coating (a) and the distribution of Ti-6Al-4V (b) after high-energy ball and SPS sintering.

The EDAX results showed prominent Ca and P peaks in Hank´s solution, while Ringer´s showed peaks of C, Cl, Si at the surface of the film. Ti-6Al-4V samples were observed in clean samples a lot of porous after sintering. Sintering process was made by SPS (Spark Plasma Sintering); materials subjected to SPS conditions displayed lower hardness and higher porosity levels [11]. It is worth mentioning that, during SPS, a pulsed current generates plasma which leads to a surface activation of the powder particles. Some researchers involved in mechanical milling with other materials (silicon with titanium), observed that the milling results showed that it was difficult to reach

a very fine and homogeneous distribution of silicon in the titanium matrix. The different diffusion progress for the dispersoid formation in dependence on the primary silicon particle size can be observed, the smaller Si particles already exhibit diffusion connected with diffusion porosity [12]. After the sintering process, a film of carbon involving the real sample was observed in Ti-6Al-4V samples (fig. 5); then samples were cut off in transversal way to find the real Ti-6Al-4V sample. Later on, SEM micrographs revealed the granular morphology of the carbon film.

### *3.2. Potentiodynamic polarization studies*

The Ti-6Al-4Vgreen samples, SPS and Commercial samples were immersed in Ringer´s and Hank´s solution. Before those samples were mechanically polished (using various grades of SiC paper), rinsed in distilled water and dried. Table 2 shows the density of the sintering samples.

**Table. 2.** Densities of nanometric samples of Ti-6Al-4V made by SPS and commercial.

| Milling intensity [h] SPS | Density |
|---|---|
| 0 | 3.8757 ± 0.085 g/cc |
| 3 | 3.8674 ± 0.017 g/cc |
| 5 | 3.9537 ± 0.025 g/cc |
| 8 | 4.3250 ± 0.017 g/cc |
| Commercial | 4.3770 ± 0.005 g/cc |

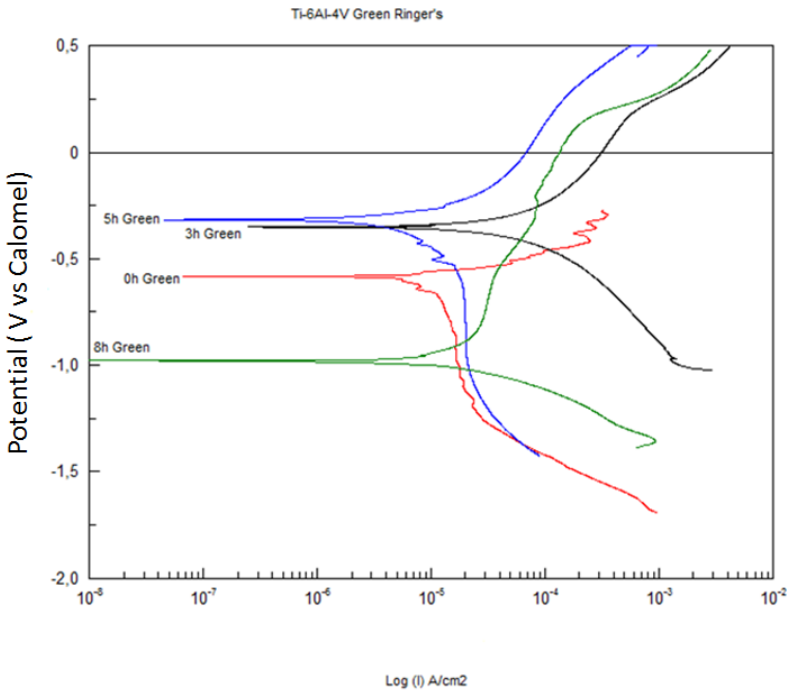


**Figure 6.** Comparison of potentiodynamic polarization curves of Ti-6Al-4V green samples in Ringer´s solution.

To understand the behavior of material as a determination of the chemical interaction of metallic materials/bone prothesis with the body fluid environment is essential in order to understand their stability in the human body. One simple way to study the film formation and passivation of implants/alloys in a solution is to monitor the Ecorr as a function of time [13].

The potentiodynamic polarization curves of Ti-6Al-4V green samples in Ringer´s solution of 0, 3, 5 and 8 h are shown in Figure 6, where the reverse scan curve of all the four different samples, indicated that they were more resistant to the pitting corrosion in Hank´s solution than Ringer´s solution. Potentiodynamic polarization curves of green samples are shown in Figure 7.

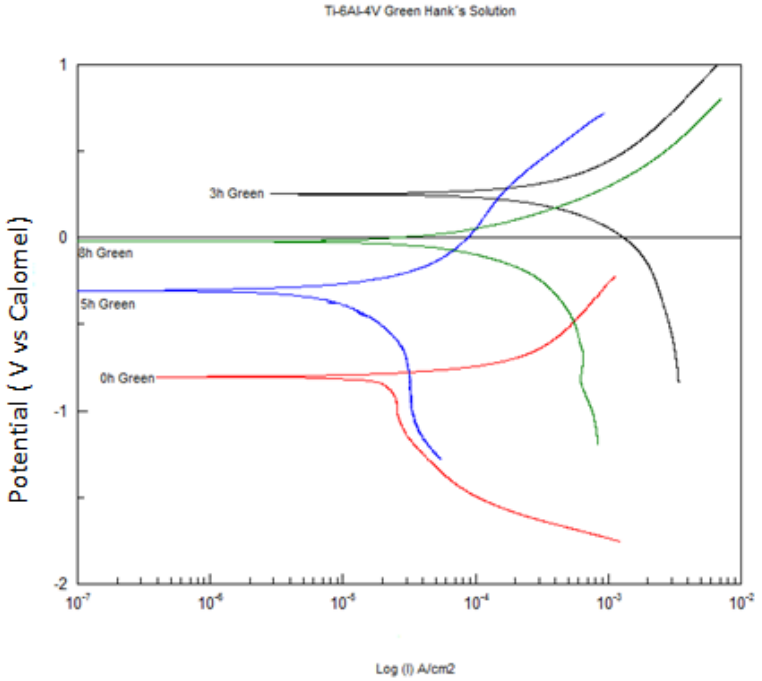


**Figure 7.** Potentiodynamic polarization curves of Ti-6Al-4V green samples in Hank´s solution.

The pitting corrosion resistance of any material/coating can be ranked based on the loop area of the cyclic polarization curves. The result of corrosion products are shown in figures 8 and 9 for Ringer´s and Hank´s solution respectively. Potentiodynamic polarization tests were performed at the scan rate of 100 mV/min, in the cathodic and anodic directions. In the cathodic direction, the potential scan was limited to 250 mV, in the anodic direction the potential was scanned up to 3000 mV from their respective OCP. Figures 10 and 11 show the potentiodynamic polarization curves in SPS samples in Ringer´s and Hank´s solution. The surface morphology after subjecting them to polarization studies are shown in figures 12 and 13, indicating that their surface was attacked and, subsequently, exhibiting some pits.

The cyclic polarization plots in Ringer´s solution and the reverse scan curve of the green and SPS sintering samples forward scan, indicated that the samples were resistant to pitting corrosion in

Ringer´s and Hank´s solution. This observation indicates that the pitting corrosion resistance of green is highly comparable to SPS, and commercial samples.

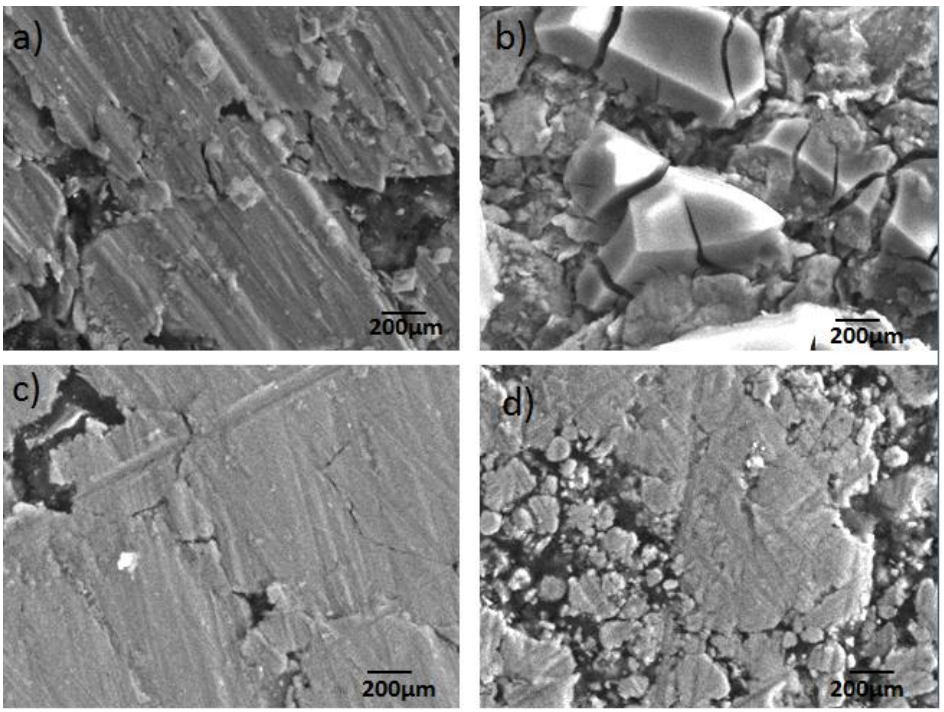


**Figure 8.** Green samples of Ti-6Al-4V (a) 0, (b) 3, (c) 5 and (d) 8h after electrochemical analysis in Ringer´s solution.

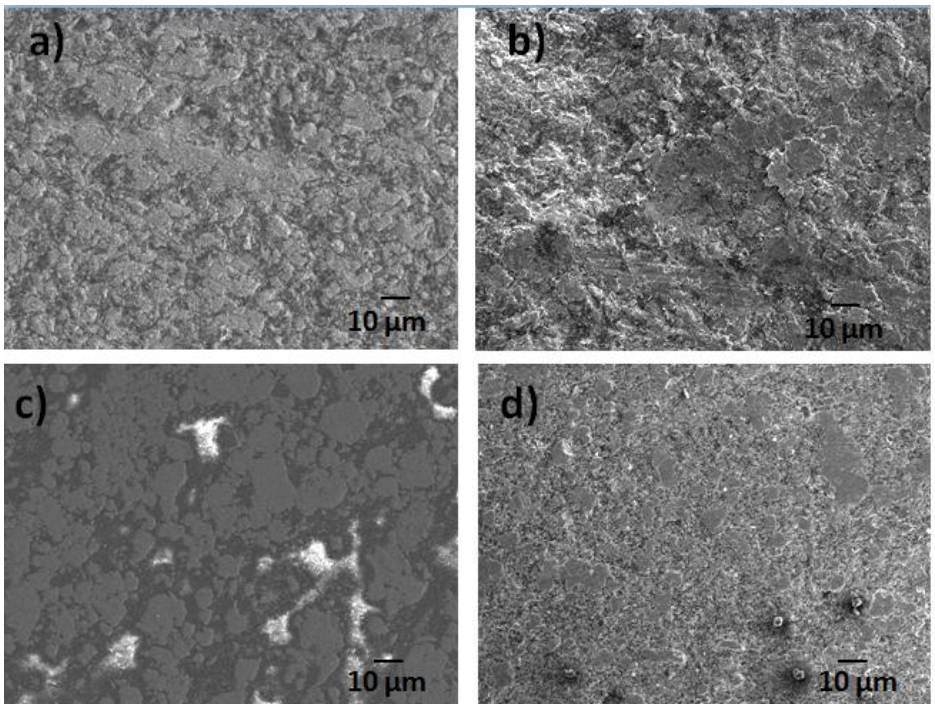


**Figure 9.** Green samples of Ti-6Al-4V(a) 0, (b) 3, (c) 5 and (d) 8h after electrochemical analysis in Hank´s solution.

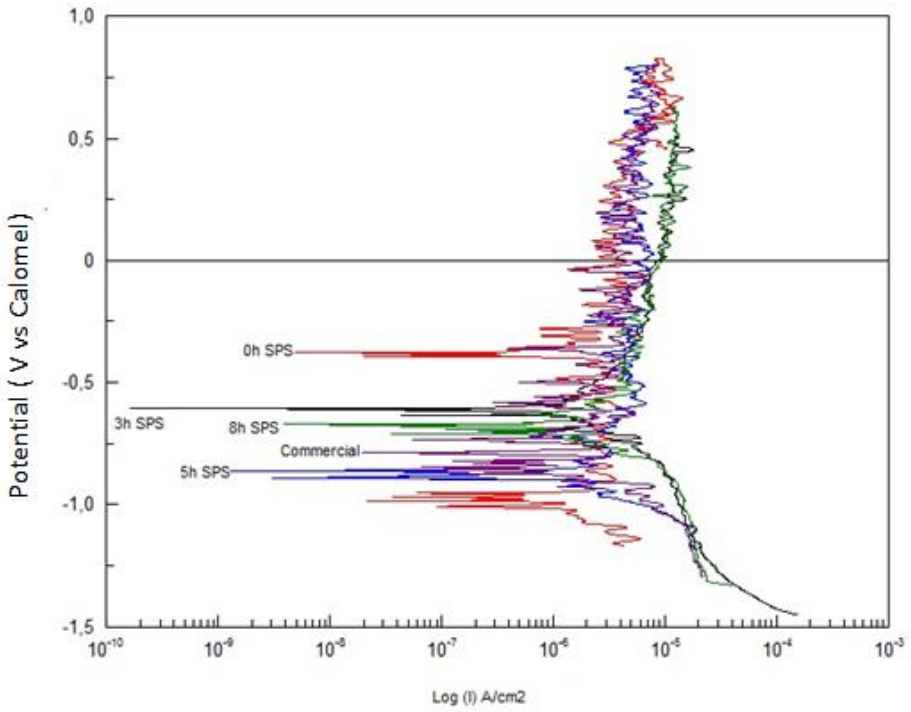


**Figure 10.** Comparison of potentiodynamic polarization curves of Ti-6Al-4V SPS and commercial alloy samples in Ringer´s solution.

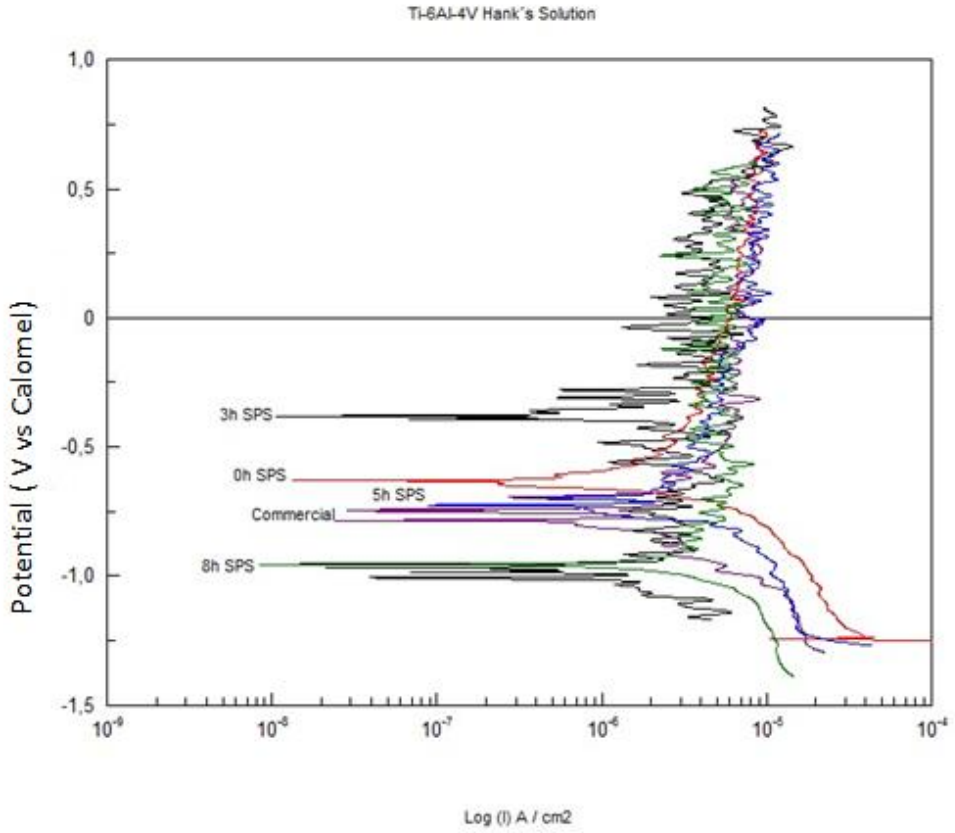


**Figure 11.** Comparison of potentiodynamic polarization curves of Ti-6Al-4V SPS and commercial alloy in Hank´s solution.

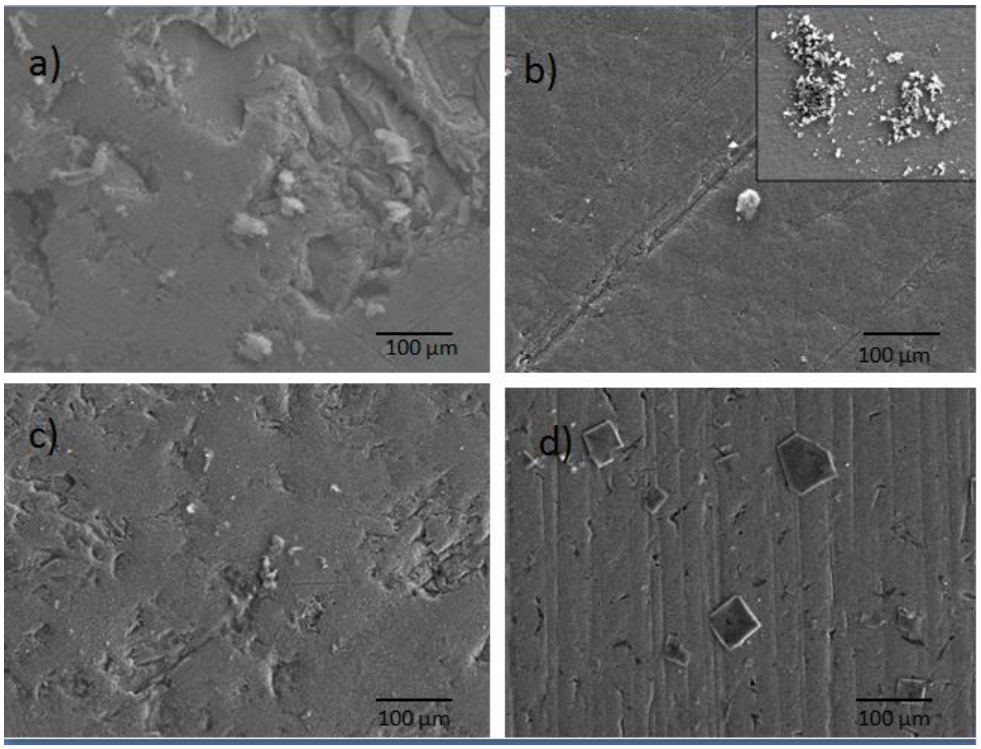


**Figure 12.** Ti-6Al-4V SPS (a) 0, (b) 5, (c) 8h and (d) commercial alloy in Ringer´s solution after potentiodynamic test.

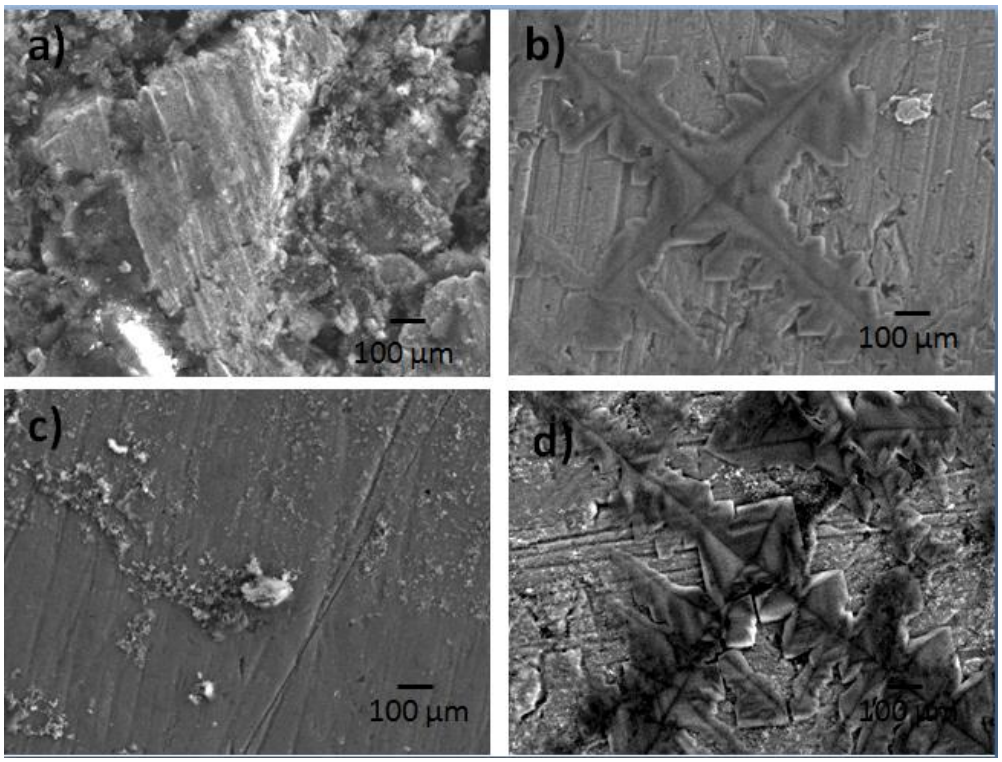


**Figure 13.** Ti-6Al-4VSPS (a) 0, (b) 5, (c) 8h and (d) commercial alloy in Hank´s solution after potentiodynamic test

*3.3. Fractal and COMSOL analysis*

Compactation pressure or sintering temperature was an important topic related to powder metallurgy, which influences each other; previous results indicates that the dimension of pores in some ternary systems decrease in the process of compacting and sintering [14].

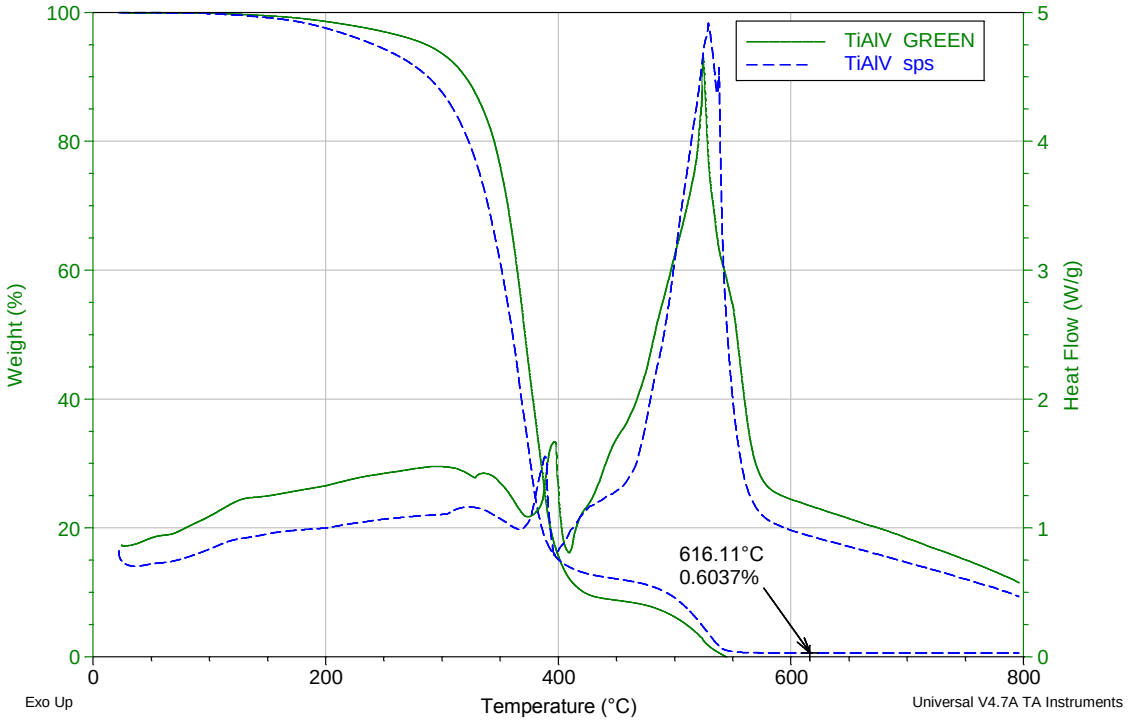


**Figure 14.** TGA results obtained for Ti-6Al-4V SPS and green encapsulated, bristles showing no thermal degradation.

The dimension of pores changed in the process of compacting and sintering, the fractal theory is a very useful tool to analyze a complicated system. To understand the differences in the potentiodynamic graphics between green powders and sintering powders, the epoxy resin was studied with a TGA (Thermogravimetric Analysis) and IR (Infrared Spectroscopy) analysis. This is intended to find the loss of mass in the resin, having the possibility of pass some resin into the Ti-6Al-4V green samples. As can be seen in figure 14, the TGA and IR analysis did not show any differences between green and sintering samples.

The microstructure of the samples from SEM was studied where the dimension of powder and pores is theoretically equal. After compacting or sintering, powders are out of shape, while the pores are isolated, whose dimensions are possible to be measured. The side length of grid is $\varepsilon$. The number of grid $N$ multiplied by $\varepsilon$ is approximate the length of the grid $L(\varepsilon)$. For a pore area, when $\varepsilon$ becomes smaller. The relationship relating the length estimate $L(\varepsilon)$ with ε given by:

$$L(\varepsilon) = M\varepsilon^{(1-D)} \quad (1)$$

where $M$ is a positive constant, $D$ is a fractal dimension, $L(\varepsilon)$ is the length of grid, $L(\varepsilon) = N\varepsilon$.

D (fractal dimension) can be detected from the slop of $lg\ N$ and $lg\ \varepsilon$. The microstructure feature and fractal dimension, $E_{corr}$ and $I_{corr}$ of green and SPS samples in Hank´s and Ringer´s solution is shown in table 3.

**Table 3.** Electrochemical and dynamical parameters in Ringer´s solution

| Type of sample Ringer's Solution | $E_{corr}$ (V) | $I_{corr}$ | $D_{F(Fractal\ Dimension)}$ |
|---|---|---|---|
| Green 0h | -0.734 | 1.380E-5 | 1.72 |
| Green 3h | -0.505 | 9.040E-7 | 1.42 |
| Green 5h | -0.164 | 3.856E-5 | 1.46 |
| Green 8h | -1.131 | 1.482E-5 | 1.22 |
| SPS 0h | -0.228 | 4.448 E-7 | 1.65 |
| SPS 3h | -0.784 | 2.890E-7 | 1.74 |
| SPS 5h | -0.708 | 4.046E-6 | 1.41 |
| SPS 8h | -0.806 | 2.178E-8 | 1.60 |
| Commercial | -0.634 | 8.642E-10 | 0.93 |

Fractal dimension describes part of the corrosion behavior. Another way to find this behavior consists in applying numerical methods, to investigate the effect of microstructure and corrosion; the heterogeneity in the porosity distribution among cultivars was visually evident from the 2-D images using fractal dimension [15, 16]. Some investigations used Arbitrary Langrangian Eulerian (ALE) application mode in COMSOL MultiPhysics, which is capable of explicit tracking the moving interface [17]. The occurrence of corrosion depends on several factors. This is why the development of an effective model is of vital importance to predict localized corrosion. Hence initiation involves analyzing several important factors for both alloy and surface. To find the initiation of corrosion in a simulated body fluid, finite element method (FEM) describes the evolution of the environment within the crevice and the impact of the geometry of the crevice [18].

The finite element method is used to solve the problem. Calculations involving the resulting of partial differential equations (PDE) were performed using COMSOL software program [19, 20]. Parameters used in the simulations corresponding at the spatial dimension of the mathematical model (run in 1D modeling), using an electrochemistry module. The geometry was created with two intervals: the electrolyte and the porous electrode.

## 4. CONCLUSIONS

- The microstructure characteristics confirm that Ti-6Al-4V alloy green samples increases their micro hardness with milling time.

- TGA studies confirm that porous in the samples did not change the structural characteristics of the epoxy resin; this means that resin did not fill the porous in green samples.
- Potentiodynamic polarization curves of Ti-6Al-4V green samples in Ringer´s solution and Hank's solution are quite similar.
- The passivation range was lower in 0h only in green samples in both solutions.
- The corrosion products found in both solutions were appropriate.
- Fractal dimension was a useful tool to understand the corrosion behavior because is correlated to the sample porous.
- Mathematical modeling via COMSOL is not comparable at all with real experimental conditions to understand corrosion behavior.

ACKNOWLEDGMENTS
This work was supported by Nanomining-263942 (FP7-NMP-2010-EU-MEXICO). The technical assistance by Victor Orozco, Adan Borunda, Enrique Torres, Karla Campos, Jair Lugo and Gregorio Vazquez is gratefully acknowledged.

**References**

1. S. Tamilselvi, V. Raman, N. Rajendran, *J.Appl Electrochem*, Springer 2009.
2. C.D.Arrieta-González, J. Porcayo-Calderon , V.M. Salinas-Bravo, J.G. Chacon-Nava , A. Martinez-Villafañe, J.G. Gonzalez-Rodriguez, , *Int. J. Electrochem. Sci.*, 6 (2011) 3644 – 3655.
3 F. Barragán, R. Guardián, C. Menchaca, I. Rosales, J. Uruchurtu, *Int. J. Electrochem*. Sci., 5 (2010) 1799 – 1809.
4. N. Zaveri, G. D. McEwen, R. Karpagavalli, A. Zhou, *J. Nanopart Res, Springer*, 2009.
5. S. Kumar, T.S.N.S. Narayanan, *J. Alloys Compd* (2009).
6. W.Y. Guo, J.Sun, J.S. Wu, *Mater. Chem. Phys*, 113 (2009) 816–820.
7. D. Gopi, V. Collins, A. Prakash, L. Kavitha, *Mat Sci Eng*, 29 (2009) 955-958
8. C. Lohoua, G. Bertrandb, *Pattern Recognition*, 40 (2007) 2301 – 2314.
9. S. H.Wang, J. Horn, H.Wang, *Opt Lasers Eng*, 46 (2008) 281–289
10. M. Cieslik, W. R. Ski, A. Janus, K. Engvall, R. Socha, A. Kotarba, *Corros. Sci.*, 51 (2009) 1157–1162.
11. K. Morsi, A. El-Desouky, B. Johnson, A. Mar and S. Lanka, *Scr Mater*, 61 (2009) 395–398.
12. D. Handtrack , F. Despang , C. Sauer, B. Kieback, N. Reinfried, Y. Grin, *Mat Sci Eng A*, 437 (2006) 423–429.
13. C.D Arrieta-Gonzalez, J. Porcayo-Calderon, V.M. Salinas-Bravo, J.G. Gonzalez-Rodriguez, J.G. Chacon-Nava, *Int. J. Electrochem*. Sci., 6 (2011) 4016 – 4031.
14. J. Kong, C. Xu, J. Li, W. Chen, H. Hou, *Adv. Powder Technol* , 22 (2011) 439-442.
15. F. Mendoza, P. Verboven, Q. Ho, G. Kerckhofs, M. Wevers, B. Nicolai, *J. Food Eng* , 99 (2010) 206–215.
16. J. Alvarez-Ramirez, J. C. Echeverria, E. Rodriguez, ", *Physica A*, 387 (2008) 6452–6462.
17. T. Hutt, P. Cawley, *NDT and E Int*., 42(2009) 141-149.
18. K. B. Deshpande, *Electrochim. Acta*, 56(2011) 1737-1745.
19. K. Yaya, Y. Khelfaoui, B.Malki, M. Kerkar, *Corros. Sci.*, 53(2011) 3309-3314
20. W. B.J. Zimmerman, *World Scientific*, 2006.